Valence photodetachment of Li^- and Na^- using relativistic many-body techniques

J. Jose,[1] G. B. Pradhan,[1] V. Radojević,[2,4] S. T. Manson,[3] and P. C. Deshmukh[1,4,*]

[1]*Department of Physics, Indian Institute of Technology Madras, Chennai-600036, India*

[2]*Institute of Physics, Pregrevica 118, P.O. Box 68, 11080 Beograd-Zemun, Serbia*

[3]*Department of Physics and Astronomy, Georgia State University, Atlanta, Georgia 30303, USA*

[4]*School of Basic Sciences, Indian Institute of Technology Mandi, Mandi 175001, India*

(Received 9 December 2010; revised manuscript received 12 March 2011; published 20 May 2011)

The multiconfiguration Tamm-Dancoff technique (MCTD) is applied to study photodetachment of negative ions of lithium and sodium. A cusplike structure is found in the photodetachment cross section just below the first detachment-plus-excitation threshold of Li^- (Li $2p$), and of Na^- (Na $3p$), in qualitative agreement with existing theoretical and experimental results. The current work emphasizes the importance of correlation in the form of configuration interaction in the photodetachment process and demonstrates the utility of MCTD in dealing with highly correlated systems.

DOI: 10.1103/PhysRevA.83.053419 PACS number(s): 32.80.Gc

I. INTRODUCTION

Photodetachment studies of anions have attracted wide interest as these processes are excellent theoretical and experimental test beds to investigate the role of important many-electron correlations. The valence electron is only weakly attached to the atom, and correlation effects are not overshadowed by the nuclear Coloumb field, i.e., correlation effects are crucial determinants of virtually all properties of negative ions. Correlation effects have, therefore, a decisive influence on photodetachment parameters [1,2]. From an applications standpoint, accurate photodetachment data are required in plasma physics, atmospheric physics, and many other fields of physics, thus enhancing the motivation to understand photodetachment dynamics of negative ions [3–5].

A number of theoretical methods that have been applied to the photabsorption process generally can also be applied to investigations of photodetachment. These methods include close coupling [6], R-matrix [7], K-matrix L^2 [8], nonrelativistic random-phase approximation (RPA) [often called RPA with exchange (RPAE)] [9], relativistic random-phase approximation (RRPA) [10], the RRPA with relaxation (RRPA-R) [11], many-body perturbation methods [12], the multiconfiguration Hartree-Fock (MCHF) technique [13], and its relativistic counterpart, the multiconfiguration Dirac-Fock (MCDF) technique [14], among others. The RRPA has been applied earlier to study dipole photodetachment of halogen negative ions [15], and this work was recently extended to investigate interchannel coupling effects on nondipole photodetachment parameters of Cl^- [16]. In addition, RRPA-R was employed to investigate relaxation and polarization effects on the photodetachment of the valence shell of Cl^- [17], and this method was subsequently used to study near-threshold relaxation effects on photodetachment of intermediate subshells of Cl^- and Br^- [18].

On the experimental side, early studies were performed on negative ions using electron scattering to form the anions [19,20], and using laser photodetachment of the anions themselves [21]. Resonances in negative ions have emerged as subjects of great interest since they are also governed by many-electron correlation effects [21–23]. Unlike the case of neutral atoms or positive ions, negative ions support only a finite number of bound states, since the effective potential of negative ions does not exhibit a long-range Coulomb tail. There have been several theoretical and experimental studies on negative-ion resonances (excited bound states) [21–23].

Over the past few decades there has been much progress in the study of the photodetachment of atomic anions [1,2,24]. In particular, several theoretical and experimental investigations have been performed on the simplest alkali-metal negative ions, Li^- and Na^-. Employing the close-coupling technique, a pronounced cusp was predicted [6] in the photodetachment cross section of valence shells of Li^- and Na^-, in the vicinity of the second detachment threshold, i.e., the photodetachment-plus-excitation channels leaving the residual alkali-metal atom in the excited np state. This prediction was confirmed in Li^- by a subsequent K-matrix L^2 basis calculation [8] as well as an R-matrix [25] calculation, which also predicted the essential features of the Li^- photodetachment cross section, in excellent agreement with previous theoretical results [6]; also for Na^-, the earlier prediction was confirmed using R-matrix methods [26,27]. An early measurement of the photodetachment cross section for Li^- and K^- in the cusp region [28] revealed no sign of the cusp, most likely owing to inadequacy of the energy resolution. Subsequently, several experiments [29–31] observed the pronounced cusp near the first detachment-plus-excitation threshold for Li^-.

The inclusion of two-electron excitation channels, detachment plus excitation in these cases, is crucial to a correct description of the photodetachment process. The multiconfiguration Tamm-Dancoff (MCTD) method [32] includes such channels, but has been applied hitherto only to a few cases, originally to the photoionization of atomic Be and Mg. Since detachment plus excitation, along with other correlation effects, are so important in negative ions, the MCTD technique offers itself as a viable methodology to these processes. Its successful application would provide a stringent test of the ability of MCTD to accurately describe many-electron correlations. Accordingly, in the present work, the photodetachment of Li^- and Na^- using the MCTD method

*Corresponding author: pcd@physics.iitm.ac.in

is studied in an environment where correlation effects are of crucial importance. Some preliminary results of the present studies have been reported earlier for the Li^- case [33].

II. THEORETICAL FRAMEWORK

The (relativistic) MCTD method applied in the present work is closely related to the RRPA [10]; the ground-state many-electron correlations are accounted for differently, while the excited (continuum) state correlations are taken into account in the same way as in the RRPA, i.e., as in the usual Tamm-Dancoff approximation [34], which does not account for the initial state correlation.

In the MCTD methodology, used earlier for calculation of photoionization of Be and Mg [32], the initial-state electron correlations are included via a multiconfiguration initial-state wave function. In the present case it was obtained using the MCDF [35] and GRASP92 [36] codes. The MCTD initial state with total angular momentum quantum numbers J,M is represented as

$$\psi(JM) = \sum_{r=1}^{n_g} c_r \phi(\gamma_r JM), \tag{1}$$

where the $\phi(\gamma_r JM)$ are configuration state functions, linear combinations of antisymmetrized products of single-particle wave functions which are eigenfunctions of J^2 and J_z, γ_r represents all other quantum numbers required to define the corresponding configuration uniquely, n_g is the number of states included, and c_r is the configuration mixing (weight) coefficient for each configuration state.

The MCTD final (excited continuum) state wave function with total angular momentum quantum numbers J',M' is taken to have the form

$$\Psi(J',M') = \sum_{i=1}^{n_c} c_i \chi(\gamma_i J'M') + \sum_{j=1}^{n_b} d_j \Phi(\gamma_j J'M'), \tag{2}$$

where $\chi(\gamma_i J'M')$ and $\Phi(\gamma_j J'M')$ are configuration state functions obtained from one of the ground-state configurations (parent configuration) by photoexciting a valence orbital a to an orbital $\bar{a}$ which is asymptotically continuum for open channels and vanishes asymptotically for closed channels (configurations χ), or to a discrete orbital (configurations Φ), respectively. The configurations Φ are constructed in the present work from the set of orbitals included in the representation of the ground state and they are referred to as excited-bound (XB) states. The last term in Eq. (2), composed of the configurations Φ, makes the expansion of the final-state wave function more complete and contains much of the short-range correlation. The parameters c_i are the weight coefficients of the parent configuration, while d_j are the weight coefficients of the XB states. The numbers n_c and n_b designate the number of the continuum (or virtually excited) configurations, i.e., number of photoionization or photodetachment channels.

The weight coefficients d_j of the XB configurations are solutions of the system of linear algebraic equations of the type used in the configuration interaction (CI) calculations,

$$\sum_{j=1}^{n_b} [H_{kj} - (E_0 + \omega)\delta_{kj}] d_j = F_k, \quad k = 1, \ldots, n_b, \tag{3}$$

where $H_{kj} = \langle \Phi(\gamma_k JM)|H|\Phi(\gamma_j JM)\rangle$ is the atomic Hamiltonian matrix element between XB configurations k and j, E_0 is the ground-state energy, ω is the photon energy, and the terms F_k are given by

$$F_k = -\sum_{i=1}^{n_c} H_{ki} c_i, \tag{4}$$

with H_{ki} being the atomic Hamiltonian matrix element between XB configuration k and a configuration corresponding to a continuum channel i.

The continuum orbital function $y_{\bar{a}}$ for an open channel (or a virtual orbital for a closed channel) created by a transition $a \to \bar{a}$ is the solution of the following radial equation, of the same type as the one used in the Tamm-Dancoff approximation,

$$(h_{\bar{a}} + V_{\bar{a}} + I_{\bar{a}} - \omega) y_{\bar{a}} = R_{\bar{a}}, \tag{5}$$

where $h_{\bar{a}}$ is the radial free-particle Dirac Hamiltonian, $V_{\bar{a}}$ is the Hartree-Fock $V(N-1)$ potential, ω is the photon energy, and $I_{\bar{a}}$ is the threshold energy of the relevant channel. Note that this differs from (single-configuration) Tamm-Dancoff and RRPA methodologies, where the threshold energies are equal to eigenvalues of single-particle orbital equations. The inhomogeneous term $R_{\bar{a}}$ describes the interchannel coupling and the coupling to XB configurations and can be written as

$$R_{\bar{a}} = C_{\bar{a}} + B_{\bar{a}} + L_{\bar{a}}, \tag{6}$$

where $C_{\bar{a}}$ describes the coupling between channels, $B_{\bar{a}}$ describes the coupling with transitions $b \to b'$ between valence orbitals leading to the XB states, and $L_{\bar{a}}$ is the term with Lagrange multipliers ensuring the orthogonality to the ground-state orbitals. The expression for the channel coupling term is

$$\begin{aligned} C_a(r) = \frac{-1}{r}\Bigg[& \frac{1}{c_{\bar{a}}} \sum_{\substack{b\bar{b}k \\ \bar{b}\neq\bar{a}}} c_{\bar{b}} A^k(\bar{a}\bar{b},ab) Y^k_{ab}(r) y_{\bar{b}}(r) \\ & + \sum_{\substack{b\bar{b}k \\ \bar{b}\neq\bar{a} \\ cfg(b)\neq cfg(a)}} A^k(\bar{a}a,\bar{b}b) Y^k_{b\bar{b}}(r) u_a(r) \\ & + \frac{1}{c_{\bar{a}}} \sum_{\substack{b\bar{b}k \\ cfg(b)\neq cfg(a)}} c_{\bar{b}} A^k(\bar{a}b,\bar{b}a) Y^k_{\bar{b}a}(r) u_b(r) \Bigg], \end{aligned} \tag{7}$$

where $A^k(ab,cd)$ are angular coefficients of the two-electron radial integrals in the expression for the total energy of the atomic system in the relevant configuration state, and Y^k_{ab} is the Hartree's Y function defined as

$$Y^k_{ab}(r) = r \int_0^\infty \frac{r^k_<}{r^{k+1}_>} u^\dagger_a(r') u_b(r') dr'. \tag{8}$$

The expression for the coupling to XB states is

$$\begin{aligned} B_{\bar{a}}(r) = \frac{-1}{r}\frac{1}{c_{\bar{a}}}\Bigg\{ & \sum_{bb'k} d_{b'} \big[A^k(\bar{a}b',ab) Y^k_{ab}(r) u_{b'}(r) \\ & + A^k(\bar{a}\bar{b},b'a) Y^k_{b'a}(r) u_b(r) \big] \\ & + \sum_{\substack{b' \\ \kappa_{\bar{b}}=\kappa_{\bar{a}}}} d_{b'} T(\bar{a}b') h_{b'} u_{b'}(r) \Bigg\}, \end{aligned} \tag{9}$$

where $\kappa_{b'} = \kappa_{\bar{a}} = \mp(j + 1/2)$ for $j = l \pm 1/2$, l and j being respective orbital and total electron angular momentum quantum numbers of an electron, and $T\left(\bar{a}b'\right)$ are angular coefficients of the single-electron radial integrals in the expression for the total energy of atomic system in the relevant configuration state. The term with Lagrange multipliers $\lambda_{\bar{a}b}$ is given by

$$L_{\bar{a}}(r) = \sum_b \lambda_{\bar{a}b} u_b(r). \tag{10}$$

The major advantage of the MCTD over the RRPA is that it can be applied to photoabsorption of open-shell atomic systems as well as to treat two-electron excitations, both ionization and detachment plus excitation and doubly excited autoionizing states.

In order to account for initial-state correlation, a CI expansion consisting of the following eight relativistic configurations to describe the initial state of the Li^- ion was employed:

$$1s^2\left(2s^2 + 2p_{1/2}^2 + 2p_{3/2}^2 + 3s^2 + 3p_{1/2}^2 + 3p_{3/2}^2 + 3d_{3/2}^2 + 3d_{5/2}^2\right), \quad J = 0.$$

Similarly, for the photodetachment study of the Na^- ion, the initial state was constructed from the following configurations:

$$1s^2 2s^2 2p^6\left(3s^2 + 3p_{1/2}^2 + 3p_{3/2}^2 + 3d_{3/2}^2 + 3d_{5/2}^2 + 4s^2\right), \quad J = 0.$$

The GRASP92 [36] package, which is an improved version of Oxford MCDF code by Grant *et al*. [35], was used to obtain the MCDF wave functions and configuration weights.

Photodetachment thresholds I_i for the various possible processes were obtained as $I_i = (E_N - E_{N-1})$, where E_N is the total energy of the N-electron negative ion (with $N = 4$ for Li^-, $N = 12$ for Na^-) in the dominant configuration among the relativistic configuration state functions (eight for Li^- and six for Na^-) included in the MCDF calculation. The one-electron orbitals obtained for the N-electron ion were used to construct $(N-1)$-electron configuration wave functions corresponding to the $(N-1)$-electron neutral atom resulting from the photodetachment of the negative ion, leaving the neutral atom in one of the eight configurations $(1s^2)2s$, $2p_{1/2}$, $2p_{3/2}$, $3s$, $3p_{1/2}$, $3p_{3/2}$, $3d_{3/2}$, $3d_{5/2}$ for the Li case; in the case of the Na^- ion, the neutral atom is left after photodetachment in one of the six configurations $(1s^2 2s^2 2p^6)3s$, $3p_{1/2}$, $3p_{3/2}$, $3d_{3/2}$, $3d_{5/2}$, $4s$. The wave functions of the $(N-1)$-electron neutral atom states were taken to be single-determinant wave functions with orbitals obtained from the initial-state calculation, in each case, much as what is done in RRPA. It must be noted, however, that not all of the single-particle orbitals are associated with physical states. Thus, for Li, the $1s^2 2s$ and $1s^2 2p_j$ wave functions do indeed represent physical states since the $2s$ and $2p_j$ are essentially spectroscopic orbitals. On the other hand, the $n = 3$ orbitals are correlation orbitals (pseudo-orbitals) so that the functions $1s^2 3l_j$ are pseudostates, included to make the expansion set for the final-state wave function more complete. Similarly, for Na, only $3s$ and $3p_j$ are essentially spectroscopic orbitals; the others are correlation orbitals.

The correlation in the final states of the systems is introduced via the (Tamm-Dancoff) coupling of channels, similar to what is done in RRPA. In any case, however, this procedure leads to energies that are sometimes inaccurate, owing to the use of the initial-state orbitals, i.e., no relaxation is included. Despite this limitation, the electron affinities (excitation energies from the negative ion to the ground state of the atom) are reasonably accurate, as indicated in Table I, as are the excitation energies of the first excited states of the atoms.

TABLE I. Threshold energies (in eV) for transitions from the negative ions Li^- and Na^- to various states of neutral Li and Na, respectively, along with experiment [29,30,37,38].

Transition	MCDF (present)	Experiment
$Li^- \rightarrow Li\ 1s^2 2s$	0.621	0.617 [29], 0.618 [30]
$1s^2 2p_{1/2}$	2.4903	2.4568 [38]
$1s^2 2p_{3/2}$	2.4904	2.4569 [38]
$Na^- \rightarrow Na\ 1s^2 2s^2 2p^6 3s$	0.544	0.547 [37]
$1s^2 2s^2 2p^6 3p_{1/2}$	2.530	2.641 [38]
$1s^2 2s^2 2p^6 3p_{3/2}$	2.532	2.643 [38]

III. RESULTS AND DISCUSSION

A. Photodetachment of Li^-

In the MCTD calculation used for Li^-, the relativistic dipole channels representing photodetachment, leaving the Li atom in the $2s$, $2p$, $3s$, $3p$, and $3d$ states, were coupled; specifically, the channels from the initial (ground) state of Li^- to the following final states (the presence of inner shell $1s^2$ is assumed in all of them),

$$\begin{gathered}
2s\varepsilon p_{1/2},\ 2s\varepsilon p_{3/2},\\
2p_{1/2}\varepsilon d_{3/2},\ 2p_{3/2}\varepsilon d_{3/2},\ 2p_{3/2}\varepsilon d_{5/2},\\
2p_{1/2}\varepsilon s,\ 2p_{3/2}\varepsilon s,\\
3s\varepsilon p_{1/2},\ 3s\varepsilon p_{3/2},\\
3p_{1/2}\varepsilon d_{3/2},\ 3p_{3/2}\varepsilon d_{3/2},\ 3p_{3/2}\varepsilon d_{5/2},\\
3p_{1/2}\varepsilon s,\ 3p_{3/2}\varepsilon s,\\
3d_{3/2}\varepsilon f_{5/2},\ 3d_{5/2}\varepsilon f_{5/2},\ 3d_{5/2}\varepsilon f_{7/2},\\
3d_{3/2}\varepsilon p_{1/2},\ 3d_{3/2}\varepsilon p_{3/2},\ 3d_{5/2}\varepsilon p_{3/2},
\end{gathered}$$

a total of 20 channels, all coupled to $J = 1$, were included. In the subsequent discussion, the $1s^2$ shall generally be omitted from the designation of states for simplicity. The resulting total photodetachment cross section is shown in Fig. 1, for the first 3 eV or so above threshold, and it is compared with several earlier theoretical [6,8,25] and experimental [28–31] results. Cross sections determined in both the length and velocity forms are presented; good agreement between length and velocity is seen. We note that some test calculations (not shown) were done with fewer configurations and continuum channels. The agreement between length and velocity forms improved as the number of configurations (and corresponding detachment channels) was increased.

There is an overall qualitative agreement between MCTD results and the earlier theoretical and experimental results, although there is unsatisfactory agreement across certain energy regions. Below the $2p$ threshold, only photodetachment leaving the Li atom in the $2s$ state is energetically possible. It is seen that just above the $2s$ threshold, the cross section

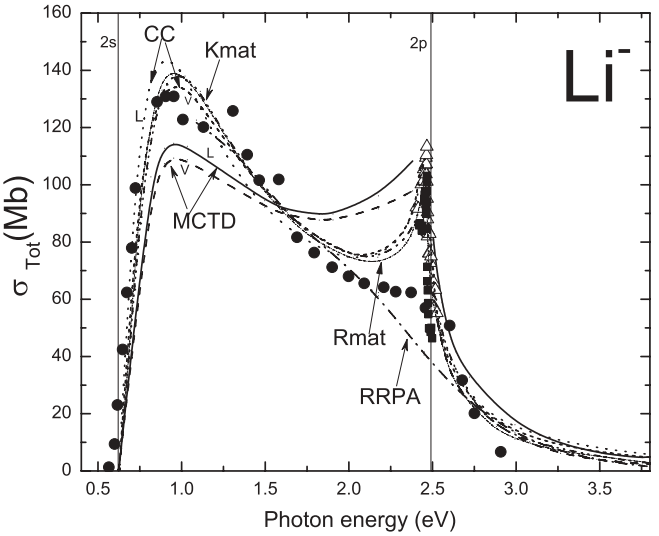

FIG. 1. Total MCTD length (L) and velocity (V) photodetachment cross sections of Li^- along with earlier close-coupling (CC) [6], *K*-matrix (Kmat) [8], and *R*-matrix (Rmat) [25] calculations and experiment (solid circles [28], open triangles [29], solid squares [30,31]). Also shown are the results of the present RRPA calculation. The vertical lines indicate the thresholds.

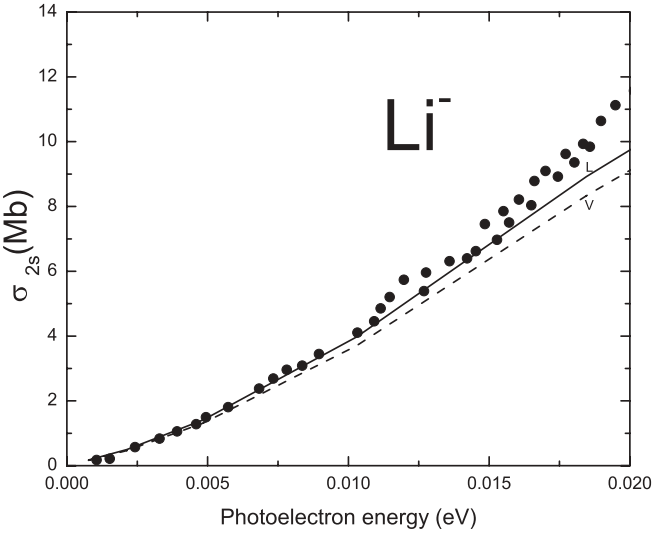

FIG. 2. MCTD length (L) and velocity (V) photodetachment cross section of Li^- near the 2*s* threshold, along with experiment (solid circles) [40].

rises rapidly from the threshold, in accordance with the Wigner threshold law [39], and in excellent agreement with experiment [28] and earlier theoretical results [6,8,25]. The cross section exhibits two maxima, a somewhat broad peak at ∼1 eV, and a sharp cusplike peak at ∼2.5 eV, and falls off rapidly above the higher-energy maximum. In the vicinity of the first maximum, MCTD lies a bit below the experimental cross section, but does lie within the experimental error bars. This first maximum is not a resonance but arises simply because photodetachment cross sections vanish at threshold and subsequently rise from zero. Above the first maximum, the cross section drops off to a minimum, but the cross section at around this minimum significantly exceeds all other results. This is likely due to the limited set of basis orbitals used to construct the wave functions in the calculations.

It is important to study the details of the MCTD result in the low-energy region, near the 2*s* threshold. In Fig. 2, the 2*s* photodetachment cross section near the 2*s* threshold is compared with experiment [40]. According to Wigner threshold law, in the low-energy region, the 2*s* cross section will be $(E-E_2s)^{3/2}$. From Fig. 2, excellent agreement between MCTD and the experimental result is seen, which suggests that the MCTD method is quantitatively accurate near threshold and upholds the Wigner threshold law.

At the higher energies, in the vicinity of the cusp, quite reasonable agreement is found with more recent experiments [29–31], but there appears to be a problem with the earlier measurement [28] which does not even show the cusp. However, it must be noted that the present MCTD calculation does not converge right at the cusp, nor within ∼0.1 eV on either side of the cusp. Thus, no comparison with experiment could be made over this small energy region.

The cusp arises from interchannel coupling between the closed part of the $2p\varepsilon s$ channels and the open $2s\varepsilon p$ channels. This Wigner cusp [39] was predicted, on very general grounds, at the opening of a photodetachment-plus-excitation channel which results in a continuum *s* wave. To emphasize the interchannel coupling nature of this cusp, we have also performed a RRPA calculation which is based on the *single* determinant wave function $1s^2 2s^2$ and, since it does not include the $2p\varepsilon s$ channels, this cusp is, of course, absent. The possibility of inclusion of such two-electron excitation channels in the MCTD method is thus a significant improvement over RRPA.

The cross section for photodetachment, leaving the Li atom in the excited 2*p* state, is shown in Fig. 3, along with the experimental result [31] and earlier calculations [8,25]. The MCTD calculation reproduces the rise from the zero value of the cross section at the Li 2*p* threshold rather well and is in reasonably good agreement with the *K*-matrix and *R*-matrix

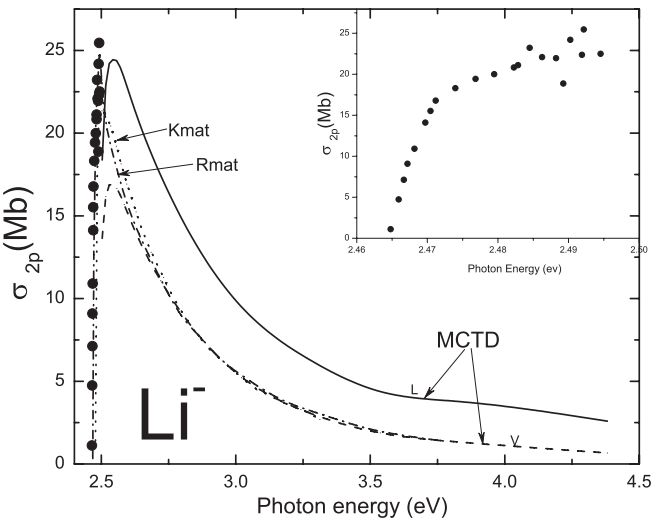

FIG. 3. Photodetachment cross section of Li^- leading to the 2*p* excited state of neutral Li. In addition to the MCTD length (L) and velocity (V) results, the earlier *K*-matrix (Kmat) [8] and *R*-matrix (Rmat) [25] cross section and experiment (solid circles) [30,31] are shown.

cross sections. In accordance with the Wigner threshold law, the $2p\varepsilon s$ channels exhibit a near-threshold photoelectron energy dependence of $\varepsilon^{1/2}$, while the $2p\varepsilon d$ channels behave as $\varepsilon^{5/2}$; thus for small ε the cross section to the Li $2p$ state is dominated by the $2p\varepsilon s$ channels. Above 2.485 eV the measurement shows (unphysical) rapid fluctuations [as seen in the inset of Fig. 3(a)] and, as a result, we do not compare with the experimental measurements above 2.485 eV.

Owing to the fact that Li^- does not support any excited bound states, all of the photoabsorption strength goes into the continuum. Then, owing to the Thomas-Reiche-Kuhn sum rule [41], the total oscillator strength in the continuum equals the number of electrons, four in this case. Since the $1s$ and $2s$ thresholds are very well separated for Li^-, to an excellent approximation, the sum rule is satisfied for each subshell individually. We have estimated the oscillator strength for the photodetachment process by integrating the area under the oscillator strength distribution curve from the photodetachment threshold up to ∼50 eV above the threshold, at which the cross section becomes vanishingly small. In the figure shown, we have plotted the cross section only up to photon energy of 4.5 eV, beyond which the cross section is small and decreases monotonically. The oscillator strength for detachment leaving the Li atom in the ground, $2s$, state was found to be 1.76 in the length form and 1.68 in the velocity form. This result suggests that most of the oscillator strength lies in the photodetachment to the Li $2s$ channel; that in the photodetachment plus excitation that would leave the Li atom in the $2p$ excited state will not be more than ∼15%.

B. Photodetachment of Na^-

In the MCTD calculation for Na^-, the relativistic dipole channels representing photodetachment, leaving the Na atom in the $3s$, $3p$, $3d$, and $4s$ states, were coupled; specifically, the channels from the initial (ground) state of Na^- to the following final states (the presence of inner shells $1s^22s^22p^6$ is assumed in all of them),

$$
\begin{aligned}
&3s\varepsilon p_{1/2},\ 3s\varepsilon p_{3/2},\\
&3p_{1/2}\varepsilon d_{3/2},\ 3p_{3/2}\varepsilon d_{3/2},\ 3p_{3/2}\varepsilon d_{5/2},\\
&3p_{1/2}\varepsilon s,\ 3p_{3/2}\varepsilon s,\\
&3d_{3/2}\varepsilon f_{5/2},\ 3d_{5/2}\varepsilon f_{5/2},\ 3d_{5/2}\varepsilon f_{7/2},\\
&3d_{3/2}\varepsilon p_{1/2},\ 3d_{3/2}\varepsilon p_{3/2},\ 3d_{5/2}\varepsilon p_{3/2},\\
&4s\varepsilon p_{1/2},\ 4s\varepsilon p_{3/2},
\end{aligned}
$$

a total of 15 channels coupled to $J = 1$, were included. The results for the total photodetachment cross section of Na^- in the threshold region are shown in Fig. 4, are compared with earlier close-coupling results [6], R-matrix results [26,27], and RPAE [42] results. Even though the quantitative agreement is not satisfactory in some energy regions, there is good overall qualitative agreement between MCTD cross sections and the earlier theoretical results. As in the Li^- case, the length and velocity forms of the MCTD cross section are close to one another throughout the energy region considered. Qualitatively, the Na^- cross section is quite similar to the case of Li^-; the rise of the cross section at threshold in accordance with Wigner threshold law [39], the broad peak just above threshold, and the sharp peak (cusp) at higher energy, just below the opening of the next detachment threshold,

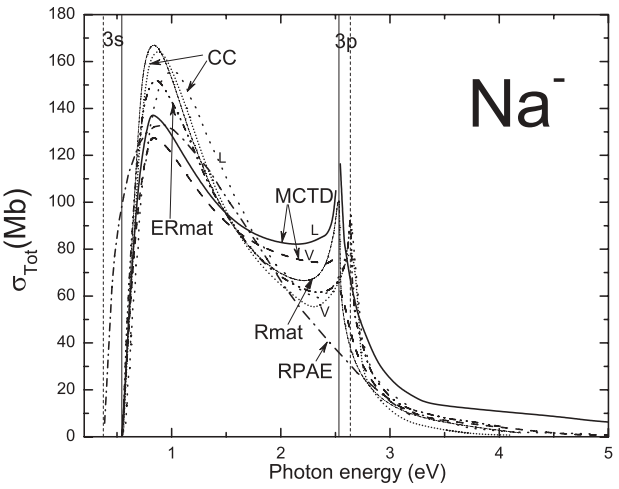

FIG. 4. Total MCTD photodetachment cross section of Na^- along with previous theoretical calculations: Close-coupling (CC) [6], eigenchannel R-matrix (ERmat) [26], R-matrix (Rmat) [27], and nonrelativistic random-phase approximation (RPAE) [42]. L and V designate length formulation and velocity formulation results. The solid vertical lines indicate the MCTD thresholds, the dashed $3s$ line is the DF threshold, and the dashed $3p$ line is the experimental threshold.

are all similar to the Li^- case. Again the cusp is due to interchannel coupling between the closed part of the $3p\varepsilon s$ channels and the open $3s\varepsilon p$ channels. A calculation performed omitting this interchannel coupling (not shown) finds no cusp, thereby substantiating the interpretation given, which is further substantiated by the results of a RPAE calculation [42], where the photodetachment-plus-excitation channels are not included. Note that, although an experimental study of Na^- photodetachment in this energy region has been reported [28], it is considered to be rather inaccurate in that its magnitudes are much below any of the theoretical calculations, and it fails to reproduce the cusp, just as was the case for Li^-.

Figure 5 shows the photodetachment cross section of Na^- leading to the $3p$ excited state of Na. Length and velocity

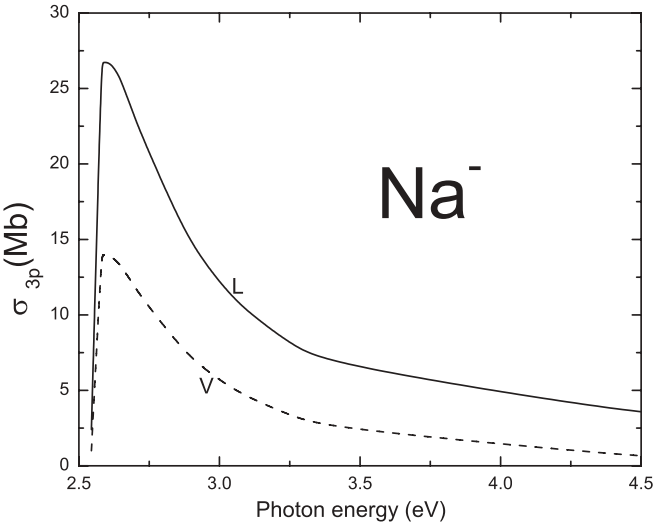

FIG. 5. Photodetachment cross section of Na^- leading to the $3p$ excited state of neutral Na in length (L) and velocity (V) formulations.

cross sections are similar to each other in shape, rising rapidly in the near-threshold region. It is seen that there is a significant discrepancy between the length and velocity results, indicating that a set of states larger than was used is required to reach agreement between them, since MCTD, unlike RRPA, is a gauge-dependent theory. Unfortunately, to the best of our knowledge, no other theoretical and/or experimental results are available for comparison in the case of the photodetachment cross section of the $3p$ photoelectron of Na^-.

Na^-, like Li^-, has no excited bound states. Thus, all of the photoabsorption oscillator strength is in the continuum. The result of a sum-rule analysis of the Na^- photodetachment cross section leading to Na $3s$ over the energy range up to ∼50 eV above the threshold, by when the cross section becomes vanishingly small, was found to be 2.10 in the length form and 1.81 in the velocity form. The length-form value is greater than 2, which implies that the MCTD approximation does not preserve the oscillator strength sum rule. However, it seems that the calculation predicts that the total oscillator strength in the photon energy region from threshold to ∼50 eV is somewhat larger for Na^- than for Li^-, but the difference is smaller than the spread between length and velocity predictions in each case. Given that, it is not clear that there *really* is an oscillator strength difference between the two cases.

IV. FINAL REMARKS

The MCTD methodology has been applied to the calculation of the photodetachment of Li^- and Na^- in the near-threshold region, and it was shown that MCTD reproduced all of the important features of these cross sections, including the Wigner cusp qualitatively; reasonable agreement with available experiment and earlier calculations was demonstrated. Furthermore, a sum-rule analysis showed that almost all of the strength of the valence photodetachment cross sections appears in the energy region close to threshold; very little oscillator strength is left for valence photodetachment at higher energies. It was also shown that the first photodetachment-plus-excitation channel, in each case, is significantly weaker than the one-electron photodetachment.

In a general sense, the present (relativistic) MCTD calculation represents a generalization of RRPA, except that initial-state correlations are introduced explicitly via a multiconfiguration wave function, and the coupling among final (continuum) states includes channels representing two-electron excitations, emission plus excitation. Further studies using MCTD are in progress in order to test its capabilities in a variety of circumstances. Based upon the results of the present and future investigations, the MCTD method will be augmented to provide more accurate results in a variety of ways.

ACKNOWLEDGMENTS

This work was partially supported by the Department of Science and Technology, Government of India, and by NSF and DOE, Office of Chemical Sciences (USA). V.R. was partially supported by the Ministry of Science of the Republic of Serbia through project No. 141029.

[1] V. K. Ivanov, Radiat. Phys. Chem. **70**, 345 (2004).
[2] V. K. Ivanov, J. Phys. B **32**, R67 (1999).
[3] H. Massey, *Negative Ions* (Cambridge University Press, London, 1976).
[4] C. M. Hall, J. Geophys. Res. **102**, 439 (1997).
[5] R. Wildt, Astrophys. J. **89**, 295 (1939).
[6] D. L. Moores and D. W. Norcross, Phys. Rev. A **10**, 1646 (1974).
[7] K. A. Berrington, P. G. Burke, M. Le Dorneuf, W. D. Robb, K. T. Taylor, and L. Vo Ky, Comput. Phys. Commun. **14**, 367 (1978).
[8] R. Moccia and P. Spizzo, J. Phys. B **23**, 3557 (1990).
[9] M. Ya Amus'ya, N. A. Cherepkov, and L. V. Cherepkov, Zh. Eksp. Teor. Fiz **60**, 160 (1971) [Sov. Phys. JETP **33**, 90 (1971)]; G. Wendin, J. Phys. B **4**, 1080 (1971); T. N. Chang and U. Fano, Phys. Rev. A **13**, 263 (1976).
[10] W. R. Johnson and C. D. Lin, Phys. Rev. A **20**, 964 (1979); W. R. Johnson, C. D. Lin, K. T. Cheng, and C. M. Lee, Phys. Scr. **21**, 409 (1980).
[11] V. Radojević, M. Kutzner, and H. P. Kelly, Phys. Rev. A **40**, 727 (1989).
[12] H. P. Kelly, Phys. Rev. **131**, 684 (1963).
[13] C. Froese Fischer, *The Hartree-Fock Method for Atoms* (Wiley, New York, 1977).
[14] I. Grant, *Relativistic Quantum Theory of Atoms and Molecules. Theory and Computation* (Springer, Berlin, 2007).
[15] V. Radojević, H. P. Kelly, and W. R. Johnson, Phys. Rev. A **35**, 2117 (1987).
[16] J. Jose, G. B. Pradhan, P. C. Deshmukh, V. Radojević, and S. T. Manson, Phys. Rev. A **80**, 023405 (2009).
[17] M. Kutzner, J. A. Robertson, and P. Pelley, Phys. Rev. A **62**, 062717 (2000).
[18] V. Radojević, J. Jose, G. B. Pradhan, P. C. Deshmukh, and S. T. Manson, Can. J. Phys. **87**, 49 (2009).
[19] J. Perel, P. Englander, and B. Bederson, Phys. Rev. **128**, 1148 (1962).
[20] A. Kasdan, T. M. Miller, and B. Bederson, Phys. Rev. A **8**, 1562 (1973).
[21] T. A. Patterson, H. Hotop, A. Kasdan, D. W. Norcross, and W. C. Lineberger, Phys. Rev. Lett. **32**, 189 (1974).
[22] S. J. Buckman and C. W. Clark, Rev. Mod. Phys. **66**, 539 (1994).
[23] L. Jiao, Y. Zhou, and Y. Wang, Phys. Rev. A **81**, 042713 (2010).
[24] T. W. Gorczyca, Radiat. Phys. Chem. **70**, 407 (2004).
[25] C. A. Rambsbottom, K. L. Bell, and K. A. Berrington, J. Phys. B **27**, 2905 (1994).
[26] C. N. Liu and A. F. Starace, Phys. Rev. A **59**, 3643 (1999).
[27] N. Vinci, D. H. Glass, K. T. Taylor, and P. G. Burke, J. Phys. B **33**, 4799 (2000).
[28] H. I. Kaiser, E. Heinicke. R. Rackwitz, and D. Feldmann, Z. Phys. **270**, 259 (1974).

[29] Y. K. Bae and J. R. Peterson, Phys. Rev. A **32**, 1917 (1985).
[30] J. Dellwo, Y. Liu, D. J. Pegg, and G. D. Alton, Phys. Rev. A **45**, 1544 (1992).
[31] J. Dellwo, Y. Liu, C. Y. Tang, D. J. Pegg, and G. D. Alton, Phys. Rev. A **46**, 3924 (1992).
[32] V. Radojević and W. R. Johnson, Phys. Rev. A **31**, 2991 (1985).
[33] J. Jose, G. B. Pradhan, V. Radojević, S. T. Manson, and P. C. Deshmukh, J. Phys. Conf. Ser. **194**, 022096 (2009).
[34] A. L. Fetter and J. D. Walecka, *Quantum Theory of Many-Particle Systems* (McGraw-Hill, New York, 1971).
[35] I. P. Grant, B. J. McKenzie, P. H. Norrington, D. F. Meyers, and N. C. Pyper, Comput. Phys. Commun. **21**, 207 (1980).
[36] F. A. Parpia, C. F. Fischer, and I. P. Grant, Comput. Phys. Commun. **94**, 249 (1996).
[37] H. Hotop and W. C. Lineberger, J. Phys. Chem. Ref. Data **14**, 1 (1985).
[38] [http://physics.nist.gov/PhysRefData/ASD/levels_form.html].
[39] E. P. Wigner, Phys. Rev. **73**, 1002 (1948).
[40] D. Feldmann, Z. Phys. A **277**, 19 (1976).
[41] H. A. Bethe and E. E. Salpeter, *Quantum Mechanics of One- and Two-Electron Atoms*, Sec. 61 (Springer, Berlin, 1957).
[42] M. Ya. Amusia, G. F. Gribakin, V. K. Ivanov, and L. V. Chernysheva, J. Phys. B **23**, 385 (1990).